Monitoring colloidal growth with holographic microscopy

Chen Wang,[1] Hagay Shpaisman,[2] Andrew D. Hollingsworth,[1] and David G. Grier[1]

[1] *Department of Physics and Center for Soft Matter Research, New York University, New York, NY 10003*
[2] *Department of Chemistry, Bar-Ilan University, Ramat-Gan 5290002, Israel*

Holographic video microscopy yields fast and accurate measurements of the size and refractive index of individual colloidal particles and therefore provides valuable and previously unavailable insights into the progress of colloidal synthesis. Holographic characterization is precise enough to track subtle changes in properties as particles age, and can be performed rapidly enough to provide feedback for process control. We demonstrate real-time holographic monitoring of colloidal growth in the synthesis of monodisperse samples of crosslinked polydimethysiloxane (PDMS) spheres. The measured increase in the most probable radius over the course of the reaction is consistent with the LaMer model for colloidal growth. The time evolution of the joint distribution of size and refractive index reveals a population of smaller, lower-density spheres. Rather than resulting from secondary nucleation, these spheres appear to have stopped growing before the synthesis ran to completion. The same analysis reveals that these PDMS particles shrink by structural relaxation after synthesis.

Colloidal synthesis typically is monitored by performing time-resolved static light scattering [1, 2], dynamic light scattering [3], or capillary hydrodynamic fractionation [4] on samples removed from the reaction vessel. These measurements offer insights into the particles' size distribution at the time of sampling, typically by comparison to models for the anticipated distribution. Here, we describe a general method for monitoring the progress of colloidal synthesis that uses holographic video microscopy to measure the radius and refractive index of individual particles. Distributions of properties compiled from such particle-resolved data reflect the true properties of the sample without *a priori* assumptions about the nature of the distributions. They therefore offer detailed insights into the mechanism of colloidal growth including the prevalence of secondary nucleation, the uniformity and reproducibility of the growth process, and the homogeneity and stability of the resulting particles. We demonstrate the capabilities of real-time holographic particle characterization by monitoring the synthesis of monodisperse samples of crosslinked polydimethysiloxane (PDMS) spheres.

Holographic particle characterization uses predictions of the Lorenz-Mie theory of light scattering [5] to analyze holographic snapshots of individual spheres [6] that are acquired with in-line holographic video microscopy [7]. The scattering pattern due to an individual sphere is identified as a center of rotational symmetry [8, 9] and then fit pixel-by-pixel for the particle's three-dimensional position, its radius, and its refractive index [6]. A typical hologram subtends a 200×200 pixel array. Each pixel has a relative noise figure of 0.009, as determined by the median-absolute-deviation (MAD) metric. Nonlinear least-squares fitting then yields the radius of a micrometer-scale sphere to within a nanometer and the refractive index with part-per-thousand precision [6, 8, 10–12], with a typical chi-squared characteristic of 1.2 ± 0.5.

Our custom-built holographic microscope [12] illuminates the sample with the collimated beam from a fiber-coupled diode laser operating at a vacuum wavelength of 447 ± 1 nm (Coherent Cube). Light scattered by a sphere interferes with the rest of the beam in the focal plane of an objective lens (Nikon Plan Apo, 100×, numerical aperture 1.45, oil immersion). The magnified interference pattern is relayed with a tube lens to a video camera (NEC TI-324A), which records its intensity at 30 frames/s with a single-frame exposure time of 100 µs. This video stream then is digitized for analysis.

Colloidal samples flow through the 86 µm × 65 µm × 15 µm observation volume in a glass channel fabricated from a microscope slide and a number 1.5 cover slip. To facilitate analysis, the colloidal dispersion must be diluted to minimize overlap of the spheres' holograms. Accurate determination of sample properties may also require additives to stabilize the sample for analysis. The diluent, moreover, must have a well-known refractive index at the laser's wavelength and at the temperature of the measurement, which can be checked with an Abbe refractometer. At a typical flow rate of 200 µm/s, data on several thousand spheres can be acquired in 5 min, thereby providing time-resolved information on the properties of the particles in the sample.

Having access to real-time particle-resolved characterization data is useful for monitoring the progress of colloidal synthesis. To demonstrate this, we use holographic characterization to monitor the growth of monodisperse spheres of polydimethylsiloxane (PDMS) with varying degrees of crosslinking. The particles are synthesized by base-catalyzed hydrolysis and copolymerization of difunctional dimethyldiethoxysilane (DMDES) and trifunctional methyltriethoxysilane (MTES) [13–15]. A mixture of DMDES (Sigma-Aldrich, 1 vol%) and MTES (Sigma-Aldrich, 4 vol%) was added into water (Millipore MilliQ, 93 vol%) and 28-30 wt% ammonium hydroxide solution (ACROS Organics, 2 vol%) to obtain a total volume of 20 ml. The error for each volume measurement is less than 1 percent. The sample was shaken vigorously with a vortexer for 4 min at room temperature to initiate nucleation, and then left to polymerize on a rotating frame at 20 rpm for up to three hours.

Starting from the initial mixing of silane monomer into

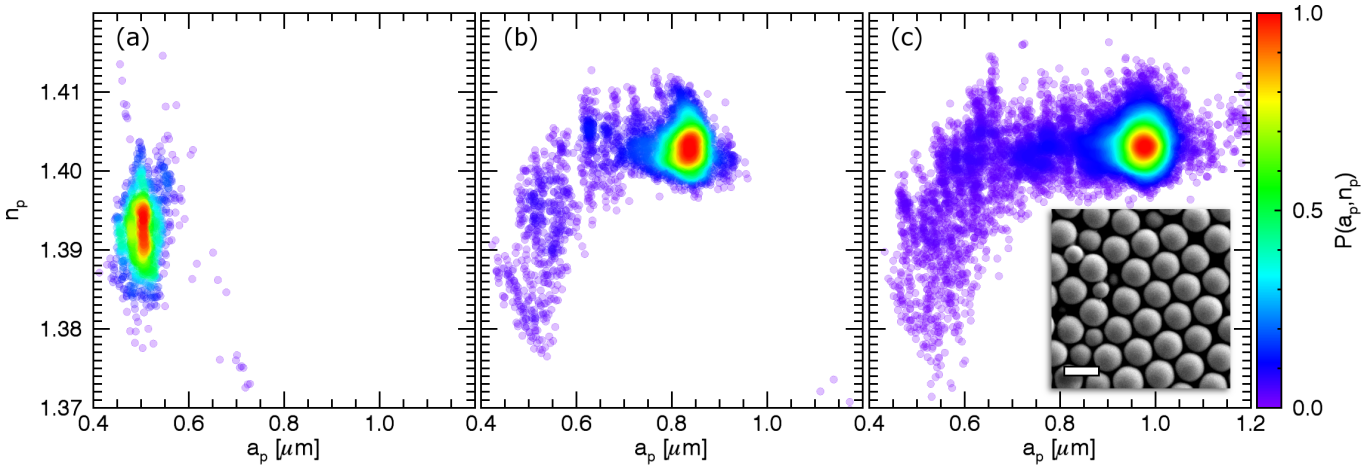

FIG. 1. Distribution of particle radius and refractive index at (a) 15 min, (b) 35 min and (c) 60 min after initiation of polymerization. Each point represents the properties of one sphere and is colored according to the relative probability density $P(a_p, n_p)$. Each plot shows the properties of 5,000 randomly selected spheres. Inset: Scanning electron micrograph of a typical sample of spheres obtained from another run of the same synthesis. Scale bar represents 2 µm.

the ammonia solution, 100 µl aliquots were taken from the reaction vessel at 15 min, 25 min, 35 min, 45 min, 60 min, and 90 min. Each aliquot was dispersed into 30 ml of 2 mM sodium dodecylsulfate (SDS) solution (Sigma-Aldrich) to dilute the sample, thereby reducing the monomer concentration enough to stabilize the spheres. The error in sampling time is estimated to be 10 s. The diluted sample then is flowed through the holographic characterization system for analysis.

The data in Fig. 1(a) through (c) show the distribution of properties of spheres measured at 15 min, 35 min and 60 min. Each plot symbol represents the radius a_p and refractive index n_p of an individual sphere, and is comparable in size to the uncertainty in the estimated parameters [6]. Symbols are colored by the joint probability density, $P(a_p, n_p)$, for observing particles with the specified properties, which is computed from the ensemble of single-particle measurements using a kernel density estimator [16].

The initial distribution in Fig. 1(a) is symmetric and quite sharply peaked in both size and refractive index. The peak of the distribution, which incorporates 90% of the particles, sharpens as the reaction proceeds and moves to larger values of refractive index and radius. This can be seen in Figs. 1(b) and 1(c). The range of refractive indexes becomes significantly smaller over the course of the reaction, which suggests that the particles in this principal population all develop to have comparable optical properties, and therefore comparable compositions. Holographic characterization is useful in this case for confirming the products' uniformity.

In addition to its principal peak, the distribution also develops a tail that traces out the reaction's history in the (a_p, n_p) plane. If this tail arose because of secondary nucleation, its shape would evolve over time because of changing reaction conditions. More likely, it reflects a

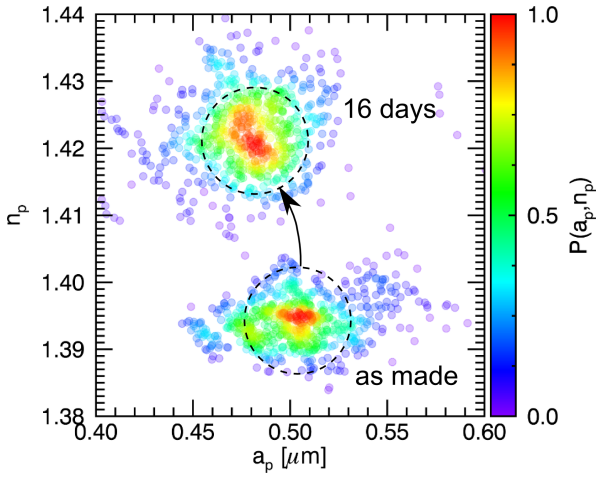

FIG. 2. Aging of PDMS particles from the sample in Fig. 1(a) extracted at 15 min. After 16 days, the mean radius has decreased and the mean refractive index has increased.

population of particles that stopped growing before fully developing.

A small population of undersized spheres is evident in the scanning electron microscope image (Carl Zeiss MERLIN) inset into Fig. 1(c). The most probable particle radius estimated from such images, 0.8 µm, is smaller than the mode radius of 0.93 µm obtained from the holographic size distribution for that batch of particles. This difference may reflect changes in the particles during drying and irradiation with the electron beam.

The distribution of size and refractive index does not change substantially between 60 min and 120 min, indicating that the reaction has run to completion. The particles' properties continue to develop, however, even after they are cleaned and resuspended in pure water. The data in Fig. 2 compare the results from Fig. 1(a)

for the size and refractive index of spheres obtained at 15 min with an equivalent measurement made on the same batch of spheres $T = 16$ d later. The diluted sample was kept sealed on a shelf under ambient conditions for the intervening period. Over this period, the most probable radius decreased from $a_p(0) = 0.50 \pm 0.01\,\mu\text{m}$ to $a_p(T) = 0.48 \pm 0.01\,\mu\text{m}$ and the most probable refractive index increased from $n_p(0) = 1.393 \pm 0.003$ to $n_p(T) = 1.420 \pm 0.003$.

These changes may be accounted for by an increase in the density, $\rho_p(t)$, of the crosslinked PDMS. The refractive index depends on $\rho_p(t)$ through the Lorentz-Lorenz relation [17]

$$L(t) \equiv \frac{n_p^2(t) - 1}{n_p^2(t) + 2} = \frac{4}{3}\pi\rho_p(t)\,\alpha, \tag{1}$$

where α is the molecular polarizability at the imaging wavelength. Because $\rho_p(t)$ is a number density, the Lorentz-Lorenz factor, $L(t)$, is dimensionless. If the density scales inversely with the spheres' volume, then we would expect the density-scaled volume

$$v(t) \equiv a_p^3(t)L(t) \tag{2}$$

to remain constant as the spheres shrink. The ratio $v(T)/v(0) = 0.95 \pm 0.08$ indeed is consistent with unity. The observed changes in size and refractive index thus are consistent with changes in polymer configuration rather than changes in composition.

The final refractive index of these early-growth spheres after aging exceeds the asymptotic value in Fig. 1(c) for spheres whose growth had run to completion. Fully grown spheres also shrink as they age, and eventually reach a stable refractive index of $n_p = 1.421 \pm 0.005$, which is consistent with the result in Fig. 2.

Were shrinkage due to elimination of solvent from void-like pores over time, the distribution $P(a_p, n_p)$ initially would exhibit an anticorrelation that would decrease as the pores shrank [18]. The absence of statistically significant correlations between a_p and n_p in either of the distributions plotted in Fig. 2 militates against this explanation. The observed shrinkage instead is better explained by densification through structural relaxation of the crosslinked polymer.

With this interpretation, the evolution of the most probable refractive index in Fig. 1 suggests that the primary nuclei are less dense than the final spheres. Whether the core density increases as the spheres grow or the low-density cores become encased in higher-density shells cannot be determined from these data. Referring again to Eq. (1), the spheres' effective density apparently changes by 2 percent over the course of the reaction.

Holographic characterization suggests that secondary nucleation does not play an important role in this reaction. The time dependence of the particle radius therefore provides information on the growth kinetics that can be used to characterize the implementation. The data in Fig. 3 show how the most probable radius increased

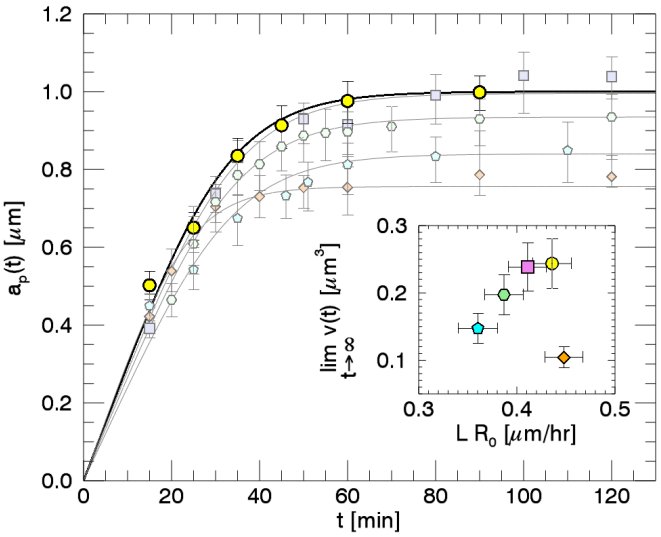

FIG. 3. Most probable radius as a function of time for five nominally identical batches of PDMS spheres at 80% crosslinker. The emphasized data set corresponds to the sample from Fig. 1. Error bars indicate the full width at half-maximum of the particle size distribution. Curves are fits to Eq. (8). Inset: Distribution of particle volumes and growth rates obtained from the fits, scaled by the Lorentz-Lorenz factors. The larger proportional range of scaled growth rates suggests that variations in nucleation efficiency account for variability in final particle size.

with time in the experiment from Fig. 1. Using conventional light-scattering techniques to obtain comparable data would have required the spheres' refractive index as an input parameter. Without an independent measurement of $n_p(t)$, such measurements would have suffered from systematic errors, particularly at early times.

The LaMer kinetic model for colloidal growth after rapid primary nucleation [19–21] assumes that each sphere grows independently in a volume V set by the number density of nuclei. As monomers are sequestered by the sphere, their number density in solution declines,

$$\rho_m(t) \approx \rho_0 - \frac{\frac{4}{3}\pi a_p^3(t)}{V}\rho_p. \tag{3}$$

For simplicity, we neglect the observed time dependence in $\rho_p(t)$, and assume that $a_p^3(t)/V$ remains small. If, furthermore, the solution around the sphere remains well mixed, then the incoming flux of monomers at the sphere's surface is limited by diffusion across a thin boundary layer,

$$\Gamma(t) = \frac{D}{\delta}\rho_m(t), \tag{4}$$

where D is the monomer diffusion coefficient and $\delta \ll V^{1/3}$ is the thickness of the boundary layer. The sphere's radius then grows as

$$\frac{da_p}{dt} = R_0\,\left[1 - \kappa^3 a_p^3(t)\right], \tag{5}$$

where the initial growth rate is

$$R_0 = \frac{D}{\delta}\frac{\rho_0}{\rho_p}, \tag{6}$$

and where the parameter

$$\kappa = \left(\frac{4\pi}{3}\frac{\rho_p}{\rho_0}\frac{1}{V}\right)^{\frac{1}{3}} \tag{7}$$

is related to the asymptotic sphere radius by $\kappa^{-1} = \lim_{t\to\infty} a_p(t)$. Equation (5) yields an implicit solution for $a_p(t)$,

$$\kappa R_0\,(t-t_0) = \frac{1}{6}\ln\left(1+\frac{3\kappa a_p(t)}{[1-\kappa a_p(t)]^2}\right) + \frac{1}{\sqrt{3}}\tan^{-1}\left(\frac{\sqrt{3}\kappa a_p(t)}{2+\kappa a_p(t)}\right), \tag{8}$$

where t_0 is the time required for nucleation. We assume that t_0 is small enough to be neglected. Curves in Fig. 3 are fits of Eq. (8) to data from five nominally identical realizations of the same synthetic protocol, including the sample from Fig. 1, with R_0 and κ as adjustable parameters.

By providing time-resolved information on both size and refractive index distributions, holographic characterization offers insights into the growth mechanism that cannot be obtained with conventional particle-characterization techniques. For example, the variability in particle size evident in Fig. 3, might reflect differences in the density of the growing microgel. Alternatively, it might be due to differences in the numbers of successful nucleation events. Holographic characterization distinguishes these scenarios.

All five runs were performed with the same initial monomer concentration, ρ_0, at the same temperature, and with the same mixing protocol. The five runs all have values of L obtained from refractive index data that are consistent with 0.243 ± 0.003. The small range suggests that the microgel grew with consistent density in each of the five samples. Using the Lorentz-Lorenz factor $L(t)$ as a proxy for the spheres' density, the scaled growth rate, $L(t)R_0 = \frac{4}{3}\pi\alpha\rho_0 D/\delta$, similarly should not vary appreciably between runs. Values of $L(t)R_0$ plotted in the inset to Fig. 3 vary by less than 10 percent relative to the mean. These observations suggest that post-nucleation growth conditions were consistent from run to run.

The asymptotic value of the normalized volume $\lim_{t\to\infty} v(t) = \kappa^{-3}L = \alpha\rho_0 V$, provides insight into the nucleation process through the number density of primary nuclei, V^{-1}. Values of $\lim_{t\to\infty} v(t)$ plotted in the inset to Fig. 3 vary by nearly 50 percent relative to the mean. Variability in mean particle size therefore may be ascribed to variations in the number density of primary nuclei, rather than differences in the density of the growing microgel. Efforts to improve reproducibility therefore should focus on improving control of the initial mixing process.

These results demonstrate that holographic characterization can be used to monitor the properties of colloidal particles both in-line as the reaction proceeds, and also after synthesis is complete to gauge stability. Although the present discussion focuses on a particular system for illustrative purposes, the same method also can be used to monitor other types of colloidal spheres synthesized by other routes, including emulsion polymerization, dispersion polymerization, and sol-gel precipitation. Holographic characterization can be performed in real time using hardware-accelerated fitting [22] or through machine-learning methods [23]. The resulting time-resolved data on the particle-size distribution is suitable for existing real-time process control systems [24]. By providing independent measurements of individual particles' sizes and refractive indexes, moreover, holographic characterization offers insights into the mechanisms of growth and aging that cannot be obtained with conventional characterization techniques. These previously unavailable data streams create new opportunities for in-line process control and quality assurance. The wealth of precise time-resolved data offered by holographic characterization, together with its low cost and ease of implementation also recommend its adoption for laboratory-scale applications.

ACKNOWLEDGMENTS

This work was supported primarily by a grant from Procter & Gamble, in part by the MRSEC Program of the National Science Foundation under Award Number DMR-1420073, and in part by NASA under grant award NNX13AR67G. Synthesis was carried out at the NYU Colloidal Synthesis Facility. The Merlin FESEM was acquired through the support of the MRI program of the National Science Foundation under Award Number DMR-0923251.

[1] A. P. Philipse, Colloid Polymer Sci. **266**, 1174 (1988)
[2] A. Becker and M. Schmidt, Macromolecular Symposia **50**, 249 (1991)
[3] R. Vacassy, R. J. Flatt, H. Hofmann, K. S. Choi, and R. K. Singh, J. Colloid Interface Sci. **227**, 302 (2000)
[4] C. A. Silebi and J. G. DosRamos, J. Colloid Interface Sci. **130**, 14 (1989)

[5] C. F. Bohren and D. R. Huffman, *Absorption and Scattering of Light by Small Particles* (Wiley Interscience, New York, 1983)M. I. Mishchenko, L. D. Travis, and A. A. Lacis, *Scattering, Absorption and Emission of Light by Small Particles* (Cambridge University Press, Cambridge, 2001)

[6] S.-H. Lee, Y. Roichman, G.-R. Yi, S.-H. Kim, S.-M. Yang, A. van Blaaderen, P. van Oostrum, and D. G. Grier, Opt. Express **15**, 18275 (2007), 0712.1738

[7] J. Sheng, E. Malkiel, and J. Katz, Appl. Opt. **45**, 3893 (2006)

[8] F. C. Cheong, B. Sun, R. Dreyfus, J. Amato-Grill, K. Xiao, L. Dixon, and D. G. Grier, Opt. Express **17**, 13071 (2009)

[9] B. J. Krishnatreya and D. G. Grier, Opt. Express **22**, 12773 (2014)

[10] K. Xiao and D. G. Grier, Phys. Rev. Lett. **104**, 028302 (2010)

[11] H. Moyses, B. J. Krishnatreya, and D. G. Grier, Opt. Express **21**, 5968 (2013)

[12] B. J. Krishnatreya, A. Colen-Landy, P. Hasebe, B. A. Bell, J. R. Jones, A. Sunda-Meya, and D. G. Grier, Am. J. Phys. **82**, 23 (2014)

[13] T. M. Obey and B. Vincent, J. Colloid Interface Sci. **163**, 454 (1994)

[14] M. I. Goller, T. M. Obey, D. O. H. Teare, B. Vincent, and M. R. Wegener, Colloids Surfaces A **123-124**, 183 (1997)

[15] Y. Saiki, C. A. Prestidge, and R. G. Horn, Colloids Surfaces A **299**, 65 (2007)

[16] B. W. Silverman, *Density Estimation for Statistics and Data Analysis* (Chapman & Hall, New York, 1992)

[17] M. Born and E. Wolf, *Principles of Optics*, 7th ed. (Cambridge University Press, Cambridge, 1999)

[18] F. C. Cheong, K. Xiao, D. J. Pine, and D. G. Grier, Soft Matter **7**, 6816 (2011)

[19] H. Reiss and V. K. La Mer, J. Chem. Phys. **18**, 1 (1950)

[20] V. K. LaMer and R. H. Dinegar, J. Am. Chem. Soc. **72**, 4847 (1950)

[21] H. Reiss, J. Chem. Phys. **19**, 482 (1951)

[22] F. C. Cheong, B. J. Krishnatreya, and D. G. Grier, Opt. Express **18**, 13563 (2010)

[23] A. Yevick, M. Hannel, and D. G. Grier, Opt. Express **22**, 26884 (2014)

[24] V. Liotta, C. Georgakis, and M. S. El-Aasser, in *Proceedings of the 1997 American Control Conference*, Proceedings of the American Control Conference, Vol. 1-6 (1997) pp. 1172–1176